



HAL
open science

Luminescent Single-Molecule Magnets as Dual Magneto-Optical Molecular Thermometers

Sophia Zanella, Maxime Aragon-Alberti, Carlos D. S. Brites, Fabrice Salles,
Luís D. Carlos, Jérôme Long

► **To cite this version:**

Sophia Zanella, Maxime Aragon-Alberti, Carlos D. S. Brites, Fabrice Salles, Luís D. Carlos, et al.. Luminescent Single-Molecule Magnets as Dual Magneto-Optical Molecular Thermometers. *Angewandte Chemie International Edition*, 2023, 62, pp.e202306970. 10.1002/anie.202306970 . hal-04239956

HAL Id: hal-04239956

<https://cnrs.hal.science/hal-04239956>

Submitted on 12 Oct 2023

HAL is a multi-disciplinary open access archive for the deposit and dissemination of scientific research documents, whether they are published or not. The documents may come from teaching and research institutions in France or abroad, or from public or private research centers.

L'archive ouverte pluridisciplinaire **HAL**, est destinée au dépôt et à la diffusion de documents scientifiques de niveau recherche, publiés ou non, émanant des établissements d'enseignement et de recherche français ou étrangers, des laboratoires publics ou privés.

Luminescent Single-Molecule Magnets as Dual Magneto-Optical Molecular Thermometers

Sofia Zanella,^{[a]#} Maxime Aragon-Alberti,^{[b]#} Carlos D.S. Brites,^[a] Fabrice Salles,^[b] Luís D. Carlos*,^[a] and Jérôme Long*^{[b][c]}

[a] S. Zanella, Pr. C. D. S. Brites, Pr. L. D. Carlos
Phantom-g, CICECO–Aveiro Institute of Materials, Physics Department, University of Aveiro, 3810-193, Aveiro, Portugal.
E-mail: lcarlos@ua.pt

[b] M. Aragon-Alberti, Dr. Fabrice Salles, Dr. J. Long
ICGM, Univ. Montpellier, CNRS, ENSCM, Montpellier, France.
E-mail: jerome.long@umontpellier.fr

[c] Dr. J. Long
Institut Universitaire de France, (IUF), 1 rue Descartes, 75231 Paris Cedex 05, France
Both authors contributed equally to this work

Supporting information for this article is given via a link at the end of the document.

Abstract: Luminescent thermometry allows the remote detection of the temperature and holds great potential in future technological applications in which conventional systems could not operate. Complementary approaches to measuring the temperature aiming to enhance the thermal sensitivity would however represent a decisive step forward. For the first time, we demonstrate the proof-of-concept that luminescence thermometry could be associated with a complementary temperature readout related to a different property. Namely, we propose to take advantage of the temperature dependence of both magnetic (canonical susceptibility and relaxation time) and luminescence features (emission intensity) found in Single-Molecule Magnets (SMM) to develop original dual magneto-optical molecular thermometers allowing to overcome the contradiction between high-performance SMM and Boltzmann-type luminescence thermometry. We highlight this integrative approach to concurrent luminescent and magnetic thermometry using an air-stable benchmark SMM [Dy(bbpen)Cl] (H₂bbpen = N,N'-bis(2-hydroxybenzyl)-N,N'-bis(2-methylpyridyl)ethyl-enediamine) exhibiting Dy³⁺ luminescence. The synergy between multiparametric magneto-optical readouts and multiple linear regression makes possible a 10-fold improvement in the relative thermal sensitivity of the thermometers over the whole temperature range, compared with the values obtained with the single optical or magnetic devices.

Introduction

The current technological demands compel the development of novel and advanced probes with remote readout to face challenges in various areas ranging from micro/nanoelectronics to photonics or biomedicine. More specifically, temperature sensors which account for 80% of the worldwide sensor market,^[1] represent imperative systems to integrate into the industry 4.0 and interneted devices. This however requires reducing the dimensions of the thermal probe at the submicrometric scale, in which conventional thermometers are ineffective while maintaining an efficient temperature determination.

In this sense, measuring the temperature (T) by monitoring the luminescence represents a remote detection spectroscopic method with a high relative thermal sensitivity ($S_T > 1\% \cdot K^{-1}$), spatial resolution ($< 10\ \mu\text{m}$) and short acquisition times ($< 1\ \text{ms}$).^[2-3] Luminescence thermometry has therefore become highly studied in recent years due to its enormous potential in nanomedicine,^[4-7] internet of things,^[8] microelectronics,^[9-11] and microfluidics.^[12]

Among the different materials that operate as luminescent thermometers, trivalent lanthanide (Ln³⁺)-based systems are attractive candidates owing to the ladder-like $4f$ level structure, sharp bandwidth emission (full width at half maximum $< 10\ \text{nm}$), long lifetimes ($> 10^{-6}\ \text{s}$), as well as photostability.^[2, 13-18] In luminescence thermometry, the thermal dependence of distinct emitting centers^[19-20] or different luminescence properties of a single emitter^[6, 21-23] have been utilized as thermometric parameters to provide self-calibrated thermometers.^[2, 24-28]

Nevertheless, luminescent thermometers might reach soon the accuracy limits needed for some applications requiring low-temperature uncertainties (δT).^[29-31] Hence, alternative approaches have now to be engineered. Combining distinct thermometric parameters to provide multiparametric sensing may overcome this issue, but to our knowledge, such an approach has solely been strictly applied to luminescent thermometers.^[30, 32-33] A complementary tool, different from luminescence, to probe the temperature would lay the foundation for dual thermometers with optimized temperature sensing and increased thermal sensitivity.

In this regard, Ln³⁺ ions could also bring additional functionality such as magnetism, which for most $4f$ ions, is characterized by a high magnetic anisotropy. Molecular chemistry concepts have been efficiently used to design original magnetic materials like Single-Molecule Magnets (SMMs).^[34-35] Such coordination complexes could be magnetized as “traditional” magnets, albeit this effect occurs at the molecular scale.^[34-36] These systems represent therefore one of the smallest magnetic memory units that could be integrated into future technologies ranging from data storage, quantum information processing, spintronics or spin valves, and transistors,^[37-42] while benefiting from all the advantages related to molecule-based materials.^[43]

In the last decade, the most performant SMMs have been extensively obtained using the exceptional magnetic properties of Dy³⁺,^[34, 36, 44-46] whereas its luminescence could be also triggered with appropriate ligands to design luminescent SMMs.^[47-51] In recent years, pioneering works have been dedicated to combining the slow relaxation of the magnetization features with luminescent thermometric

sensing.^[52-57] The magnetic properties being greatly dependent on the temperature, the local tracking of thermal changes appears pivotal.^[41, 51] Yet, there are, to our knowledge, no performant zero-field SMMs acting as highly sensitive optical thermometers (Table S1). Besides the chemical challenge of designing high-performance luminescent SMMs, a conceptual limitation needs to be further overcome. High-energy barrier SMMs require indeed large crystal-field (CF) splitting for their ground multiplet, which is also transposed in their excited emitting multiplet (${}^4F_{9/2}$ for Dy^{3+}). For Boltzmann-type luminescent thermometers,^[23] this compromises a high relative thermal sensitivity in the whole temperature window where the slow relaxation is observed as the temperature sensing window increases with the rising of the energy gap between the ground and first excited states of the emitting level.^[23, 56, 58] As SMMs are candidates for future single-molecule applications, doping with a different Ln^{3+} ion could hardly be viewed as a viable strategy. Hence, new tactics to enhance the thermal sensitivity in single emitting molecular thermometer with SMM feature appears essential. In this sense, we envision that both luminescent and magnetic properties are intimately correlated to the $4f$ electronic structures of the Ln^{3+} ions and by extension to the temperature. Indeed, the temperature affects the transitions responsible for the luminescence whereas magnetism is entirely correlated to the effect of thermal fluctuation on the spins. More specifically, the temperature dependence of $4f$ - $4f$ electronic transitions in lanthanide-based materials could be somehow compared to rules governing the magnetic properties. Paramagnetic materials were previously reported as temperature sensors based on the thermal dependence of the magnetic susceptibility.^[59-61] Taking into account the Curie law ($\chi = C/T$ with χ being the magnetic susceptibility and C the Curie constant), such systems exhibit only a significant sensitivity at very low temperatures. Furthermore, one of the signatures of an SMM is its relaxation dynamics, which is characterized by the relaxation time, τ , and which accounts for the average time needed for the magnetization of the system to randomly flip due to thermal fluctuations. This implies that both, the magnetic susceptibility and the relaxation time, might be exploited to sense the temperature and provide a complementary approach to luminescence thermometry. We hereby investigate the luminescence thermometry of an air-stable SMM for which the magnetic features outperform those of any SMM luminescent thermometer reported so far. To overcome the abovementioned limitations inherent to such Boltzmann-type thermometer, we additionally propose as a proof-of-concept to employ two different temperature sensing techniques to design multiparametric thermometers with a relative thermal sensitivity one order of magnitude larger than that achieved by each method. Hence, this unprecedented dual magneto-luminescent molecular temperature sensor allows employing up to three different parameters to improve the thermal sensitivity, which enables the measurement of the temperature over a large range (12-300 K).

Results and Discussion

To support this, a benchmark air-stable $[Dy(bbpen)Cl]$ (**1**) SMM ($H_2bbpen = N,N'$ -bis(2-hydroxybenzyl)- N,N' -bis(2-methylpyridyl)ethylenediamine)) was selected since *i*) it shows interesting magnetic properties with an anisotropic barrier close to 500 cm^{-1} and opening of a hysteresis loop,^[62] *ii*) it displays high thermal stability up to 600 K and is robust against solvent loss; *iii*) it could be synthesized in large scale, *iv*) although not previously investigated for the Dy^{3+} analogue, the $bbpen^{2-}$ is known to act as sensitizer towards various Ln^{3+} ions with relatively high quantum yield.^[63]

The complex $[Dy(bbpen)Cl]$ (**1**) was synthesized using a slightly modified synthetic procedure (see experimental section).^[62] X-ray diffraction, in line with other analyses, confirms the purity of the sample (Figure S1 in Supporting Information). The seven-coordinated complex exhibits a distorted pentagonal bipyramid geometry (Figure 1a). The coordination sphere of the Dy^{3+} is made of two phenoxide oxygens in axial positions and four nitrogen atoms belonging to the $bbpen^{2-}$ ligand, a chloride ion completing the coordination sphere of the Dy^{3+} in the equatorial plane. The crystal packing (Figure S2) analysis reveals that the shortest intermolecular Dy^{3+} - Dy^{3+} is about 8.50 Å.

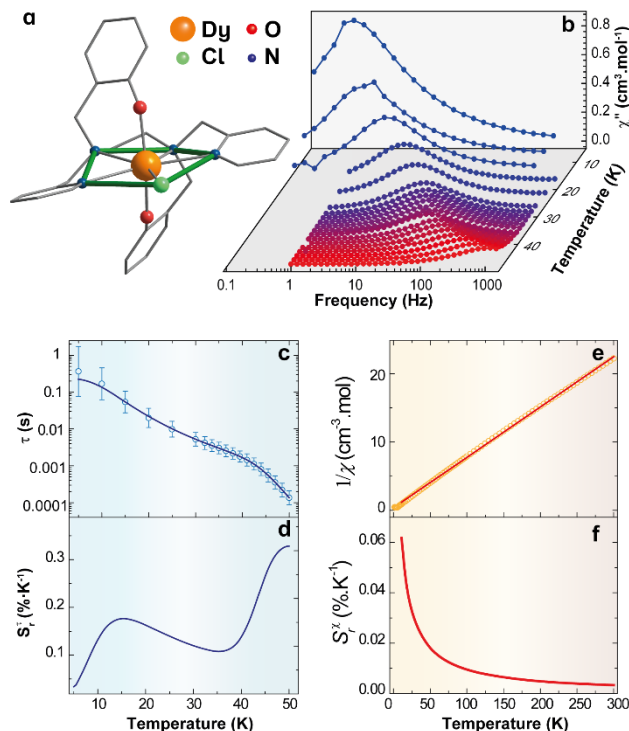


Figure 1. (a) Crystal structure of **1**. The grey bars represent the carbon atoms, and the hydrogen atoms have been omitted for clarity. (b) Frequency dependence of the out-of-phase (χ'') susceptibility for **1** under a zero dc-field. (c) Temperature dependence (5-50 K) of τ under a zero-dc field. The uncertainties were determined from the CC-FIT2 software^[64] while the solid lines correspond to the fit with Eq. 1 (0 Oe). (d) S_τ^T thermal sensitivity obtained from τ using the fitting to Eq.1. (e) Temperature dependence (2-300 K) of the inverse magnetic susceptibility, $1/\chi$, measured under a 1000 Oe dc field. The red solid line corresponds to the fit with a Curie law; $r^2 > 0.999$, for $T > 10$ K. (f) S_χ^T thermal sensitivity obtained from the inverse susceptibility.

The magnetic properties were investigated in both direct current (dc, Figure S3) and alternate current (ac) modes confirming the typical slow relaxation of the magnetization as previously evidenced (see details in the SI). In particular, the ac measurements reveal a single-temperature-dependent peak of the out-of-phase susceptibility (χ'') that could be observed up to 50 K (Figure 1b and Figures S4-S5). The relaxation dynamics was investigated by analyzing the thermal dependence of the relaxation time (Figure 1c) which reveals the characteristic shape for SMMs showing overlap of different relaxation processes. Whereas the relaxation dynamics follows a thermally activated behavior in the high-temperature range, the curvature points out the presence of Raman relaxation possibly associated with Quantum Tunnelling of the Magnetization (QTM). The thermal dependence of the relaxation could be modeled using the following equation:

$$\frac{1}{\tau} = \frac{1}{\tau_0} \exp\left(\frac{\Delta}{k_B T}\right) + C_1 T^n + \frac{1}{\tau_{QTM}} \quad (\text{Eq. 1})$$

in which the first term accounts for a thermally activated process (k_B = Boltzmann constant, Δ = effective anisotropy barrier), while the second and third ones stand for two-phonon Raman (C_1 and n being the Raman coefficient and exponent respectively) and QTM processes, respectively. To avoid over-parameterization, the n exponent was successively fixed to different values until getting the best coefficient correlation. The best-fitting parameters are: $\Delta = 656 \pm 2 \text{ cm}^{-1}$, $\tau_0 = (1.03 \pm 0.04) \times 10^{-12} \text{ s}$, $n = 3.7$, $C_1 = (6.33 \pm 0.04) \times 10^{-4} \text{ s}^{-1} \cdot \text{K}^{-n}$ and $\tau_{QTM} = 0.24 \pm 0.09 \text{ s}$. The n exponent value suggests an increased Raman relaxation with respect to that observed in dysprosium metallocenes ($n \approx 2$).^[65-66] The higher relaxation barrier in comparison with a previous study (*i.e.* 492 cm^{-1})^[62] could be explained by our fitting procedure over the whole temperature range as opposed to the linear fit only in the high-temperature region. The Δ value appears therefore much in line with a relaxation proceeding through the third excited Kramers doublets (KD) based on previously reported Complete Active Space Self Consistent Field (CASSCF) *ab initio* calculations.^[62] Additionally, we conducted such calculations followed by second-order N-Electron perturbation theory (NEVPT2) to account for dynamic correlation effects and provide a more accurate picture of the CF splitting. Comparatively, the CF splitting is found slightly larger (Table S3). The g tensor values and transition matrix elements rather suggest a relaxation through the second excited KD located at 607 cm^{-1} (Figure S6).

The relaxation dynamics is a fingerprint of the SMM behavior and τ varies by about three orders of magnitude in the investigated temperature range. We therefore propose to define τ as a thermometric parameter. As several thermometric parameters will be considered in this study, the corresponding relative thermal sensitivity (S_τ) could be calculated attending to the definition^[2]:

$$S_r^Q = \frac{1}{Q} \left| \frac{\partial Q}{\partial T} \right| \quad (\text{Eq. 2})$$

where Q denotes the thermometric parameter, that is either the relaxation time (τ), the inverse of the magnetic susceptibility ($1/\chi$) or, as discussed below, the intensity ratio Δ_T for the luminescent thermometer.

The calculated relative thermal sensitivity ascribed to τ , S_r^τ , is shown in Figure 1d and shows the presence of a maximum at about 15 K followed by a steep rise as the temperature increases to reach a value of about 0.3 % K⁻¹. It should be emphasized that the fitting of the thermal dependence of τ using Eq. 1 implies that **1** operates as a primary thermometer.

The related temperature uncertainty could be estimated from the uncertainty in the thermometric parameter Q using:

$$\delta T = \frac{1}{S_r^Q} \frac{\delta Q}{Q} \quad (\text{Eq. 3})$$

where $\delta Q/Q$ is the relative uncertainty on each of the thermometric parameters. Calculations using the standard deviations extracted from the CC-FIT2 software^[64] based on a log-normal distribution, yields however unrealistic δT values. Yet, considering the standard deviations on the relaxation time (simple fit of the generalized Debye model) gives δT of 0.4 K at low temperature (Figure S7) but reduced values of less than 0.1 K are reached in the thermally activated region.

The thermal sensitivity S_r^τ in the presence of a magnetic field was also studied (Figures S8-S12, see SI for details) and results in its enhancement for temperatures lower than 20 K.

This original approach opens tremendous perspectives since the thermometric performances could be modulated depending on the relaxation dynamics of the SMM. To illustrate this, we applied the same rationale to another SMM presenting fall-apart relaxation dynamics and anisotropic barriers: [Dy(acac)₃(H₂O)₂]·H₂O ($\Delta = 95$ cm⁻¹).^[57] It turns out it exhibits a sensitivity up to 0.8 %·K⁻¹ (Figure S13) but only in a very low-temperature range (< 12 K) in which the slow relaxation could be observed.

Remarkably, a complementary magnetic thermometric parameter for **1** could be further considered using the inverse of the magnetic susceptibility ($1/\chi$, Figure 1e) obtained from standard dc measurements and which could be fitted, due to the large CF splitting, down to 10 K with a simple Curie law ($1/\chi = T/C$). The corresponding relative sensitivity, S_r^χ , is shown in Figure 1f and confirms that sensitivity values greater than 0.06 %·K⁻¹ could be achieved exclusively in the low-temperature range (< 15 K), as previously observed in simple paramagnetic salts. This contrasts with the thermal variation of S_r^τ for which the maximum value is attained in the thermally activated region (between 40 and 50 K), confirming the asset provided by the slow relaxation of the magnetization.

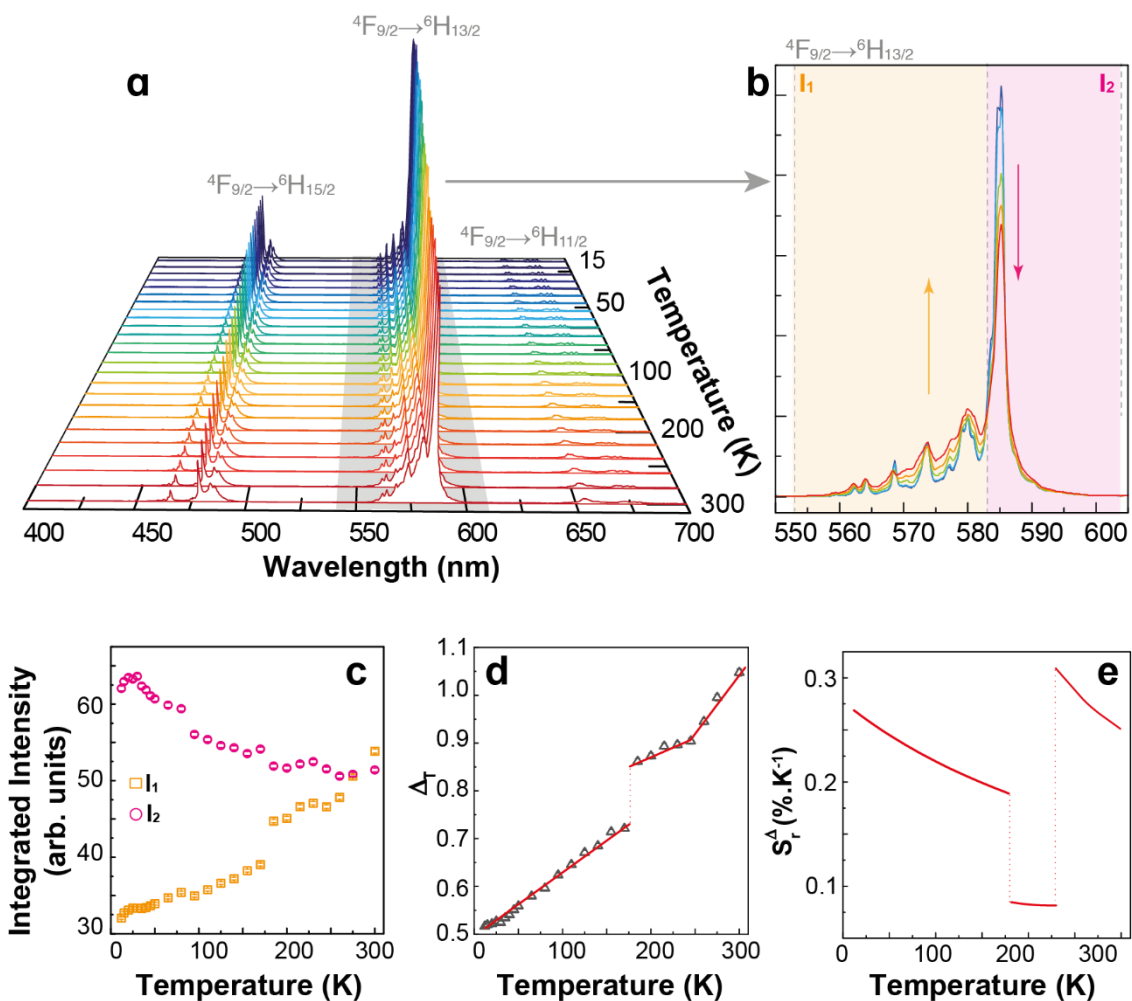


Figure 2. (a) Emission spectra of **1** (12-300 K) upon 312 nm excitation. (b) Magnification of the ${}^4F_{9/2} \rightarrow {}^6H_{13/2}$ transition displaying the temperature dependence of the high- (I_1) and low-energy (I_2) components. The integration ranges for I_1 and I_2 are shadowed. Temperature dependence of (c) I_1 and I_2 integrated areas, (d) ΔT thermometric parameter, and (e) S_T^Δ relative thermal sensitivity. In d) the data points were empirically fitted to straight lines ($r^2 > 0.976$).

We then study the luminescence thermometry of this dysprosium SMM. The excitation spectra of **1** (12-300 K), monitoring the ${}^4F_{9/2} \rightarrow {}^6H_{13/2}$ transition, displays the ligand broadband, ranging from 250 to 450 nm, overlapped with intra-4f Dy^{3+} transitions (Figure S14). The spectra are virtually temperature independent (details on the determination of the integrated area and corresponding uncertainty in Supporting Information). The emission spectra of **1** (Figure 2a) reveal the characteristic Dy^{3+} ${}^4F_{9/2} \rightarrow {}^6H_{11/2,13/2,15/2}$ transitions. For temperatures above 170 K, the ${}^4I_{15/2} \rightarrow {}^6H_{15/2}$ transition could be discerned at 450 nm, although with very small intensity avoiding its use for luminescence thermometry (Figure S15). The three ${}^4F_{9/2} \rightarrow {}^6H_{11/2,13/2,15/2}$ transitions display an analogous temperature dependence (Figure S16). Therefore, we selected the main ${}^4F_{9/2} \rightarrow {}^6H_{13/2}$ transition as representative of the luminescent thermometric features of **1** due to its larger signal-to-noise ratio, corresponding to a smaller temperature uncertainty. The emission spectra reveal more lines than the seven expected KD of the ${}^6H_{13/2}$ multiplet (Figure 2b) suggesting the contribution of excited ${}^4F_{9/2}$ levels, as previously observed.^[57] *Ab initio* calculations for Ln^{3+} excited states remain particularly intricate.^[67-68] Although the energy of the ${}^4F_{9/2}$ state is overestimated by our CASSCF/NEVPT2 calculations, the CF of the ${}^4F_{9/2}$ multiplet might be viewed as indicative. It reveals the presence of two low-lying KD estimated at 80 and 120 cm^{-1} (Table S6). In this regard, the excitation and emission spectra of **1** could be used to confirm the CF splitting of the emitting ${}^4F_{9/2}$ state (Figure S17). Yet, we will not detail the CF splitting and the origin of each component of the ${}^4F_{9/2} \rightarrow {}^6H_{13/2}$ transition assuming, instead, that the low- and high-energy sides arise, respectively, from the ground (shadowed area I_2) and excited (shadowed area I_1) ${}^4F_{9/2}$ KD (Figure 2b). Consequently, we define the thermometric parameter $\Delta T = I_1/I_2$, where the integrated intensities I_1 and I_2 range from 555 to 582.9 nm and 582.9-605 nm, respectively. The wavelength superior (inferior) limit of I_1 (I_2) corresponds to the first value for which the intensity at 300 K is not the higher value among all the spectra (Figure 2b). The I_1 and I_2 temperature dependences are presented in Figure 2c whereas Figure 2d presents the calibration curve of **1** ($\Delta T(T)$) in which three distinct linear operating ranges are discerned (Table S7).

Although a complete explanation of this empirical dependence lies outside the scope of this study, we notice the temperature associated with the transition between the first (second) to the second (third) regime matches exactly the onset of the population of the ground (first) KD of the ${}^4I_{15/2}$ multiplet (around 170 K and 220 K, respectively, Figure S15).

The relative thermal sensitivity of the luminescent thermometer (S_r^A) ranges from 0.1 to 0.3 %·K⁻¹ (12-300 K); maximum value at 225 K (Figure 2e). These values are of the order of magnitude of those reported for Ln³⁺ complexes in this temperature range.^[2] However, this constitutes, to our knowledge, the first example of a high-performance SMM ($\Delta > 600$ cm⁻¹ and opening of the hysteresis loop) exhibiting luminescence thermometry features (Table S1, Figure S18). The temperature uncertainty in the distinct operating intervals ranges from 0.4 to 2.4 K (Figure S19).

These results pinpoint that Boltzmann-type thermometers are unable to operate in the whole temperature window where the slow relaxation is observed. To illustrate this, the temperature range at which the Boltzmann-type thermometer can operate was calculated considering the first excited KD of the ⁴F_{9/2} multiplet ($\Delta E = 80$ cm⁻¹, with respect to the KD ground state obtained by CASSCF/NEVPT2 calculations). Based on the theoretical work by Suta and Meijerink,^[23] a Boltzmann-type thermometer should exhibit an optimum thermal sensitivity for $r = \Delta E/k_B T$ values comprised between 2 and $2 + \sqrt{2}$. The optimum window for 1 is found between 34 and 57 K, which only partially overlaps that of the SMM feature (Figure S20). More particularly, the low-temperature region (< 10 K) in which the opening of the hysteresis loops is detected, could theoretically not be probed using Boltzmann thermometry. To our knowledge, this is the first time that such limitation is pinpointed in SMMs. Consequently, new strategies to simultaneously enlarge the temperature windows and increase the sensing technique are needed.

With this in hands, the presented integrative approach exhibits several benefits brought by the dual thermometric sensing provided by magnetism and luminescence. Firstly, a comparison between luminescence and slow relaxation sensing indicates that the maximum thermal sensitivity is achieved in different temperature windows. Whereas luminescence sensing provides a maximum relative thermal sensitivity S_r^A of 0.3%·K⁻¹ at 225 K, the magnetic thermometry S_r^T exhibits a similar value but in the Orbach region (40-50 K) under a zero magnetic field. This unravels that these two different sensors could operate in a complementary fashion allowing cross-check temperature readings.

Besides, we propose that these two sensing techniques might not only operate independently but act synergistically. Hence, the temperature-dependent luminescence and magnetic properties of this SMM can be combined with multiple linear regression (MLR) to improve the relative thermal sensitivity of the dual magneto-optical thermometer. The data analytics now represents indeed a critical aspect in luminescent thermometry and may provide future improvements in the field, as recently highlighted.^[69-71] Although the combination of MLR and distinct temperature-dependent luminescence readouts have been recently proposed for green fluorescent protein (GFP) and Ag₂S nanoparticles (by some of us),^[30] and in all-optical thermometry of nanodiamonds with silicon-vacancy,^[72] this is the first example that applies the MLR concept to distinct properties of a particular system (Figure 3). As $\tau(T)$ is not linear over the whole temperature range (5-45 K, Figure 1c), we propose to apply the MLR methodology considering $\ln(\tau)$ for which a pseudo-linear regime could be identified (12-45 K, Figure S21). Therefore, we use $1/\chi$, Δ_T , and $\ln(\tau)$, as the two former parameters also present linear dependences on the temperature in these ranges (Figure 1e and Figure 2d, respectively). Although $1/\chi$ is collected under a 1000 dc field, this low magnetic field should not induce significant changes in the luminescence spectra caused by a Zeeman splitting and which usually requires a magnetic field of the order of several Tesla to be experimentally observed.^[52, 57] Thus, the temperature can be predicted by:

$$T = \beta_0 + \beta_1 1/\chi + \beta_2 \Delta_T + \beta_3 \ln(\tau) \quad (\text{Eq. 4})$$

where β_0 is the intercept and β_{1-3} are the slopes of the $1/\chi$, Δ_T and $\ln(\tau)$ thermometric parameters, respectively.

It turns out that for distinct temperature ranges, we have available different thermometric parameters that may be combined to calculate the temperature. While in the 12-45 K interval $1/\chi$, Δ_T and $\ln(\tau)$ are active, in the 45-300 K range only two of the three thermometric parameters are operative, and $1/\chi$ and Δ_T ($\beta_3=0$, Figure 3a), respectively. The corresponding values of the fitting parameters for all temperature ranges are presented in SI (Table S8). The donut charts (Figure 3b) represent the relative weight of each slope for the temperature change $T - \beta_0$,^[73] pinpointing that the magnetic and optical measurements are weighted distinctly in each temperature interval. The MLR allows to reach an overall relative thermal sensitivity^[30] up to 28 ± 2 %·K⁻¹ at 12 K (11 ± 1 %·K⁻¹ at 300 K, Figure 3c). This is by far the highest value reported for SMMs (one order of magnitude larger than the typical values, Table S1 and Figure S18),^[52-56] being also much higher than the great majority of the values reported for luminescent thermometers^[74-75] (although lower than the actual record obtained for Ag₂S dots, 50%·K⁻¹ at 295 K^[30]). Moreover, in the whole temperature range, there is a global increase of S_r of the dual magneto-optical thermometer relatively to the values obtained using a single thermometric parameter (Figure 1f and Figure 2e). This increase is comparable to that reported by Maturi *et al.*^[30] using MLR analysis applied exclusively to luminescent thermometers. The temperature uncertainty resulting from the MLR analysis (details in SI) increases with the temperature, being naturally lower for the temperature ranges of higher relative thermal sensitivity. The lowest temperature uncertainty, 0.1 K, is registered at 12 K (0.3 K at 300 K, Figure S23). The accuracy of the dual magneto-optical sensor (defined as the difference between the temperature values calculated using Eq. 4 and those measured in the calibration curves, Figure 2d) are presented in Figure 3d as normalized violin plots to permit a quick graphical inspection of the agreement. The accuracy values are better than 0.2 K, with $1/\chi$, Δ_T , and $\ln(\tau)$, and 0.5 K, with $1/\chi$ and Δ_T .

Finally, to demonstrate that our rationale could be applied to any paramagnetic luminescent material, additional MLR analysis was carried out considering only $1/\chi$ and Δ_T . A significant enhancement of S_r by more than one order of magnitude (14 ± 1 %·K⁻¹ at 12 K) is achieved in a large temperature range (12-300 K), relative to the values obtained considering each parameter separately (Table S9 and Figure S23). This highlights the advantage of using MLR to improve the performance of the dual magneto-optical thermometer.

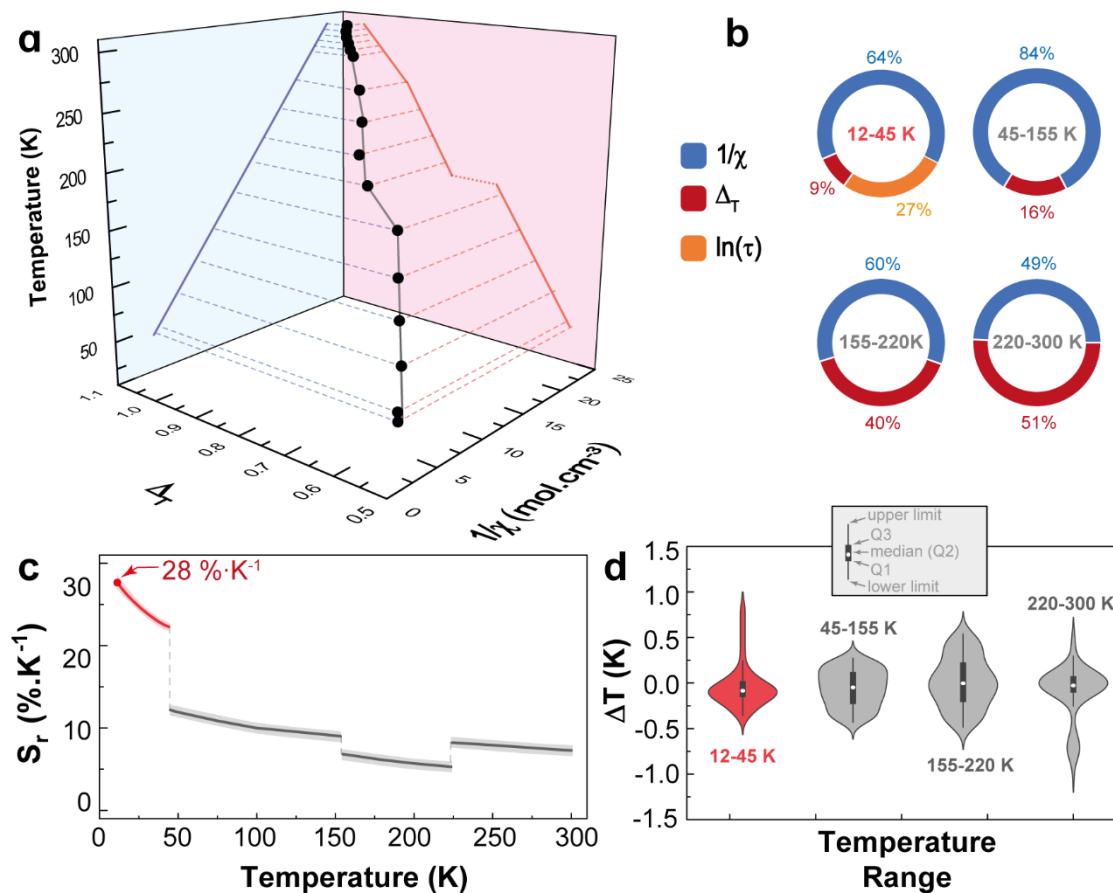


Figure 3. (a) 3D scatter plot of the temperature expressed as a function of $1/\chi$ under a 1000 Oe dc field and $\Delta\tau$. The black dots account for the MLR experimental points whereas the black line is the corresponding fit. The blue and red panels correspond to the plots presented in Figures 1e and 2d, respectively. (b) Donut charts of β -weights considered for MLR in the different temperature ranges. (c) Relative thermal sensitivity obtained through MLR in the 12-45 (red), 45-155, 155-220, and 220-330 K (grey) intervals. The shadowed areas are the corresponding uncertainties resulting from the propagation of the uncertainty on the fitting parameters ($\leq 2\% \cdot K^{-1}$). (d) Violin plots (normalized widths) of the difference between the temperature measured using the calibration curve and the calculated value through Eq. (4).

Conclusions

We demonstrated in this study that the field of SMM is not only restricted to magnetic-related or quantum-based applications but could be extended towards innovative sensors such as molecular thermometric devices. For the first time, the luminescence thermometry of a SMM exhibiting a high anisotropic barrier and magnetic bistability which clearly outperforms those of other reported SMM luminescent thermometers has been investigated. By employing a benchmark air-stable SMM we additionally demonstrated, as a proof-of-concept, that luminescence-based thermometry could be efficiently combined with a second temperature sensing tool related to a different property such as magnetism to design dual magneto-optical molecular thermometers.

In contrast to previous studies in which the SMM magnetic properties were never exploited for sensing the temperature, we further illustrated that both, the characteristic slow relaxation dynamics of a SMM as well as its canonical magnetic susceptibility, could be leveraged as thermometric magnetic parameters and complementary tools to luminescence thermometry. We subsequently show that taking the optical and magnetic data independently offers up to a threefold parametric approach that allows these sensing tools to act synergistically. Whereas both optical and magnetic thermometric performances taken individually are found below a practical threshold limit for the relative thermal sensitivity of $1\% \cdot K^{-1}$, our data analytics result in an enhanced overall thermal sensitivity which is found boosted by one order of magnitude, switching the system into a highly performant thermometer. Thus, high sensitivity up to $28\% \cdot K^{-1}$ could be reached in the cryogenic range where all the thermometric parameters are active. This clearly surpasses the thermometric performances reported so far for any SMMs using luminescence thermometry. More generally, the proposed methodology overcomes the paradigm of SMM Boltzmann-type thermometers which are intrinsically operative in a narrow temperature range, partially overlapping that of the slow relaxation window.

We emphasize that this integrative approach could be extended to other SMMs. Remarkably, the high diversity in the relaxation dynamics of luminescent SMMs would ultimately allow to rationally improve the sensitivity for their incorporation in future devices, in

which both the magnetic and luminescent properties could be collected synchronously; the main current limitation of our approach being indeed the independent acquisition of the magnetic and luminescence data. Although challenging, this could be performed using standard SQUID magnetometers or Hall magnetometers using optical fibers.^[76-77] To overcome the acquisition of three different thermometric parameters, we demonstrate that taking only the magnetic susceptibility and luminescence still generates a significant enhancement of the thermal sensitivity over the whole temperature range. In a broader context, this implies that such remote dual magneto-optical sensing is not narrowed to SMMs and could be extended to any luminescent materials exhibiting a paramagnetic behavior.

Acknowledgements

The authors thank the University of Montpellier, CNRS and PAC of ICGM. J. L. also acknowledges the support from the Institut Universitaire de France. This work has been supported by ANR with grant number ANR-19-CE07-0026-01. The France/Portugal bilateral actions Campus France/FCT PESSOA (47823YE) and CNRS International Emerging Action are also acknowledged. This work was also developed within the scope of the projects CICECO-Aveiro Institute of Materials, UIDB/50011/2020, UIDP/50011/2020 & LA/P/0006/2020, financed by Portuguese funds through the FCT/MEC (PIDDAC), The Shape of Water (PTDC/NAN-PRO/3881/2020) and LogicALL (PTDC/CTM-CTM/0298/2020). SZ also acknowledges FCT for a PhD grant (SFRH/BD/144239/2019). We thank the reviewers whose suggestions helped to greatly improve the manuscript.

Keywords: Single-Molecule Magnets • Luminescence • Molecular Thermometers • Dysprosium

- [1] Market Research Report, Grand View Research, Inc., San Francisco, **2015**.
- [2] C. D. S. Brites, S. Balabhadra, L. D. Carlos, *Adv. Opt. Mater.* **2019**, *7*, 1801239.
- [3] D. Jaque, F. Vetrone, *Nanoscale* **2012**, *4*, 4301-4326.
- [4] M. Xu, X. Zou, Q. Su, W. Yuan, C. Cao, Q. Wang, X. Zhu, W. Feng, F. Li, *Nat. Comm.* **2018**, *9*, 2698.
- [5] N. Inada, N. Fukuda, T. Hayashi, S. Uchiyama, *Nature Protocols* **2019**, *14*, 1293-1321.
- [6] Y. Shen, H. D. A. Santos, E. C. Ximendes, J. Lifante, A. Sanz-Portilla, L. Monge, N. Fernández, I. Chaves-Coira, C. Jacinto, C. D. S. Brites, L. D. Carlos, A. Benayas, M. C. Iglesias-de la Cruz, D. Jaque, *Adv. Funct. Mater.* **2020**, *30*, 2002730.
- [7] R. Piñol, J. Zeler, C. D. S. Brites, Y. Gu, P. Téllez, A. N. Carneiro Neto, T. E. da Silva, R. Moreno-Loshuertos, P. Fernandez-Silva, A. I. Gallego, L. Martinez-Lostao, A. Martínez, L. D. Carlos, A. Millán, *Nano Lett.* **2020**, *20*, 6466-6472.
- [8] J. Ramalho, S. F. H. Correia, L. Fu, L. L. F. Antonio, C. D. S. Brites, P. S. Andre, R. A. S. Ferreira, L. D. Carlos, *Adv Sci (Weinh)* **2019**, *6*, 1900950.
- [9] C. D. S. Brites, P. P. Lima, N. J. Silva, A. Millan, V. S. Amaral, F. Palacio, L. D. Carlos, *Front. Chem.* **2013**, *1*, 9.
- [10] O. A. Savchuk, J. J. Carvajal, C. Cascales, J. Massons, M. Aguiló, F. Díaz, *J. Mater. Chem. C* **2016**, *4*, 6602-6613.
- [11] J. Drabik, L. Marciniak, *ACS Appl. Mater. Interfaces* **2021**, *13*, 1261-1269.
- [12] R. G. Geitenbeek, J. C. Vollenbroek, H. M. H. Weijgertze, C. B. M. Tregouet, A.-E. Nieuwelink, C. L. Kennedy, B. M. Weckhuysen, D. Lohse, A. van Blaaderen, A. van den Berg, M. Odiijk, A. Meijerink, *Lab on a Chip* **2019**, *19*, 1236-1246.
- [13] J. Zhou, J. L. Leano, Jr., Z. Liu, D. Jin, K. L. Wong, R. S. Liu, J. G. Bunzli, *Small* **2018**, *14*, e1801882.
- [14] J. Rocha, C. D. S. Brites, L. D. Carlos, *Chem. Eur. J.* **2016**, *22*, 14782-14795.
- [15] Y. Zhou, B. Yan, *Nanoscale* **2015**, *7*, 4063-4069.
- [16] A. M. Kaczmarek, Y.-Y. Liu, M. K. Kaczmarek, H. Liu, F. Artizzu, L. D. Carlos, P. Van Der Voort, *Angew. Chem. Int. Ed.* **2020**, *59*, 1932-1940.
- [17] L. Marciniak, A. Pilch, S. Arabasz, D. Jin, A. Bednarkiewicz, *Nanoscale* **2017**, *9*, 8288-8297.
- [18] C. Hazra, A. Skripka, S. J. L. Ribeiro, F. Vetrone, *Adv. Opt. Mater.* **2020**, *8*, 2001178.
- [19] J. Periša, Z. Ristić, V. Đorđević, M. Sekulić, T. Dramićanin, Ž. Antić, M. D. Dramićanin, *J. Lumin.* **2021**, *238*, 118306.
- [20] X. Qiu, Q. Zhou, X. Zhu, Z. Wu, W. Feng, F. Li, *Nat. Comm.* **2020**, *11*, 4.
- [21] Z. Cao, X. Wei, L. Zhao, Y. Chen, M. Yin, *ACS Appl. Mater. Interfaces* **2016**, *8*, 34546-34551.
- [22] L. Marciniak, K. Prorok, L. Francés-Soriano, J. Pérez-Prieto, A. Bednarkiewicz, *Nanoscale* **2016**, *8*, 5037-5042.
- [23] M. Suta, A. Meijerink, *Adv. Theory Simul.* **2020**, *3*, 2000176.
- [24] C. D. S. Brites, P. P. Lima, N. J. O. Silva, A. Millán, V. S. Amaral, F. Palacio, L. D. Carlos, *Nanoscale* **2012**, *4*, 4799-4829.
- [25] E. J. McLaurin, L. R. Bradshaw, D. R. Gamelin, *Chem. Mater.* **2013**, *25*, 1283-1292.
- [26] Y. Cheng, Y. Gao, H. Lin, F. Huang, Y. Wang, *J. Mater. Chem. C* **2018**, *6*, 7462-7478.
- [27] M. Jia, Z. Sun, M. Zhang, H. Xu, Z. Fu, *Nanoscale* **2020**, *12*, 20776-20785.
- [28] C. D. S. Brites, A. Millán, L. D. Carlos, in *Handbook on the Physics and Chemistry of Rare Earths, Vol. 49* (Eds.: B. Jean-Claude, P. Vitalij K), Elsevier, **2016**, pp. 339-427.
- [29] J. Zhou, B. del Rosal, D. Jaque, S. Uchiyama, D. Jin, *Nat. Methods* **2020**, *17*, 967-980.
- [30] F. E. Maturi, C. D. S. Brites, E. C. Ximendes, C. Mills, B. Olsen, D. Jaque, S. J. L. Ribeiro, L. D. Carlos, *Laser Photonics Rev.* **2021**, *15*, 2100301.
- [31] M. Suzuki, T. Plakhotnik, *Biophys. Rev.* **2020**, *12*, 593-600.
- [32] J. Liu, X. Yue, Z. Wang, X. Zhang, Y. Xu, *J. Mater. Chem. C* **2020**, *8*, 13328-13335.
- [33] Y. Jiang, Y. Tong, S. Chen, W. Zhang, F. Hu, R. Wei, H. Guo, *Chem. Eng. J.* **2021**, *413*, 127470.
- [34] D. N. Woodruff, R. E. P. Winpenny, R. A. Layfield, *Chem. Rev.* **2013**, *113*, 5110-5148.
- [35] R. A. Layfield, M. Murugesu, *Lanthanides and Actinides in Molecular Magnetism*, Wiley, **2015**.
- [36] J.-L. Liu, Y.-C. Chen, M.-L. Tong, *Chem. Soc. Rev.* **2018**, *47*, 2431-2453.
- [37] R. Sessoli, D. Gatteschi, A. Caneschi, M. A. Novak, *Nature* **1993**, *365*, 141-143.
- [38] L. Bogani, W. Wernsdorfer, *Nat. Mater.* **2008**, *7*, 179-186.
- [39] J. Luzon, R. Sessoli, *Dalton Trans.* **2012**, *41*, 13556-13567.
- [40] F. Troiani, M. Affronte, *Chem. Soc. Rev.* **2011**, *40*, 3119-3129.
- [41] S. Thiele, F. Balestro, R. Ballou, S. Klyatskaya, M. Ruben, W. Wernsdorfer, *Science* **2014**, *344*, 1135-1138.
- [42] G. Serrano, L. Poggini, M. Briganti, A. L. Sorrentino, G. Cucinotta, L. Malavolti, B. Cortigiani, E. Otero, P. Sainctavit, S. Loth, F. Parenti, A.-L. Barra, A. Vindigni, A. Cornia, F. Totti, M. Mannini, R. Sessoli, *Nat. Mater.* **2020**, *19*, 546-551.
- [43] D. W. Bruce, D. O'Hare, R. I. Walton, *Molecular Materials*, Wiley, **2011**.
- [44] J. D. Rinehart, J. R. Long, *Chem. Sci.* **2011**, *2*, 2078-2085.
- [45] L. Ungur, L. F. Chibotaru, *Inorg. Chem.* **2016**, *55*, 10043-10056.

- [46] A. Gould Colin, K. R. McClain, D. Reta, G. C. Kragoskow Jon, A. Marchiori David, E. Lachman, E.-S. Choi, G. Analytis James, R. D. Britt, F. Chilton Nicholas, G. Harvey Benjamin, R. Long Jeffrey, *Science* **2022**, 375, 198-202.
- [47] F. Pointillart, O. Cadour, B. Le Guennic, L. Ouahab, *Coord. Chem. Rev.* **2017**, 346, 150-175.
- [48] J. Long, Y. Guari, R. A. S. Ferreira, L. D. Carlos, J. Larionova, *Coord. Chem. Rev.* **2018**, 363, 57-70.
- [49] J. Long, *Front. Chem.* **2019**, 7, 63.
- [50] J.-H. Jia, Q.-W. Li, Y.-C. Chen, J.-L. Liu, M.-L. Tong, *Coord. Chem. Rev.* **2019**, 378, 365-381.
- [51] R. Marin, G. Brunet, M. Murugesu, *Angew. Chem. Int. Ed.* **2021**, 60, 1728-1746.
- [52] D. Errulat, R. Marin, D. A. Gállico, K. L. M. Harriman, A. Pialat, B. Gabidullin, F. Iikawa, O. D. D. Couto, J. O. Moilanen, E. Hemmer, F. A. Sigoli, M. Murugesu, *ACS Central Science* **2019**, 5, 1187-1198.
- [53] G. Brunet, R. Marin, M.-J. Monk, U. Resch-Genger, D. A. Gállico, F. A. Sigoli, E. A. Suturina, E. Hemmer, M. Murugesu, *Chem. Sci.* **2019**, 10, 6799-6808.
- [54] J. Wang, J. J. Zakrzewski, M. Heczko, M. Zychowicz, K. Nakagawa, K. Nakabayashi, B. Sieklucka, S. Chorazy, S.-i. Ohkoshi, *J. Am. Chem. Soc.* **2020**, 142, 3970-3979.
- [55] J. Wang, J. J. Zakrzewski, M. Zychowicz, V. Vieru, L. F. Chibotaru, K. Nakabayashi, S. Chorazy, S.-i. Ohkoshi, *Chem. Sci.* **2021**, 12, 730-741.
- [56] A. A. Kitos, D. A. Gállico, N. Mavragani, R. Castañeda, J. O. Moilanen, J. L. Brusso, M. Murugesu, *Chem. Commun.* **2021**, 57, 7818-7821.
- [57] R. A. S. Ferreira, E. Mamontova, A. M. P. Botas, M. Shestakov, J. Vanacken, V. Moshchalkov, Y. Guari, L. F. Chibotaru, D. Luneau, P. S. Andre, J. Larionova, J. Long, L. D. Carlos, *Adv. Opt. Mater.* **2021**, 9, 2101495.
- [58] R. Marin, D. A. Galico, R. Gayfullina, J. O. Moilanen, L. D. Carlos, D. Jaque, M. Murugesu, *J. Mater. Chem. C* **2022**, 10, 13946-13953.
- [59] F. G. Brickwedde, *J. Res. Natl. Bur. Stand. A Phys. Chem.* **1960**, 64A, 1, 1-4.
- [60] R. Soulen Jr, *Cryogenics* **1974**, 14, 250-252.
- [61] D. S. Betts, D. T. Edmonds, B. E. Keen, P. W. Matthews, *J. Sci. Instrum.* **1964**, 41, 515-516.
- [62] J. Liu, Y.-C. Chen, J.-L. Liu, V. Vieru, L. Ungur, J.-H. Jia, L. F. Chibotaru, Y. Lan, W. Wernsdorfer, S. Gao, X.-M. Chen, M.-L. Tong, *J. Am. Chem. Soc.* **2016**, 138, 5441-5450.
- [63] L. E. d. N. Aquino, G. A. Barbosa, J. d. L. Ramos, S. O. K. Giese, F. S. Santana, D. L. Hughes, G. G. Nunes, L. Fu, M. Fang, G. Poneti, A. N. Carneiro Neto, R. T. Moura, R. A. S. Ferreira, L. D. Carlos, A. G. Macedo, J. F. Soares, *Inorg. Chem.* **2021**, 60, 892-907.
- [64] D. Reta, N. F. Chilton, *Phys. Chem. Chem. Phys.* **2019**, 21, 23567-23575.
- [65] M. Briganti, F. Santanni, L. Tesi, F. Totti, R. Sessoli, A. Lunghi, *J. Am. Chem. Soc.* **2021**, 143, 13633-13645.
- [66] E. Garlatti, A. Chiesa, P. Bonfà, E. Macaluso, I. J. Onuorah, V. S. Parmar, Y.-S. Ding, Y.-Z. Zheng, M. J. Giansiracusa, D. Reta, E. Pavarini, T. Guidi, D. P. Mills, N. F. Chilton, R. E. P. Winpenny, P. Santini, S. Carretta, *J. Phys. Chem. Lett.* **2021**, 12, 8826-8832.
- [67] L. Ungur, L. F. Chibotaru, *Chem. Eur. J.* **2016**, 23, 3708-3718.
- [68] J. Jung, M. Atanasov, F. Neese, *Inorg. Chem.* **2017**, 56, 8802-8816.
- [69] E. Ximendes, R. Marin, L. D. Carlos, D. Jaque, *Light. Sci. Appl.* **2022**, 11, 237.
- [70] J. F. Silva, J. Maria de Oliveira, W. F. Silva, A. C. Costa Soares, U. Rocha, N. Oliveira Dantas, E. Alves da Silva Filho, M. Duzzioni, A. Helmut Rulf Cofré, O. Wagner de Castro, L. Anhezini, A. Christine Almeida Silva, C. Jacinto, *Chem. Eng. Sci.* **2022**, 264, 118153.
- [71] Y. Yang, L. Li, H. Suo, P. Li, Z. Wang, Z. Zhang, *Opt. Express* **2022**, 30, 265-274.
- [72] S. Choi, V. N. Agafonov, V. A. Davydov, T. Plakhotnik, *ACS Photonics* **2019**, 6, 1387-1392.
- [73] R. Piedmont, *Encyclopedia of Quality of Life and Well-Being Research; Michalos, AC, Ed* **2014**, 381.
- [74] A. Nexha, J. J. Carvajal, M. C. Pujol, F. Díaz, M. Aguiló, *Nanoscale* **2021**, 13, 7913-7987.
- [75] M. T. Abbas, N. Z. Khan, J. Mao, L. Qiu, X. Wei, Y. Chen, S. A. Khan, *Mater. Today Chem.* **2022**, 24, 100903.
- [76] C. Min, J. Park, J. K. Mun, Y. Lim, J. Min, J.-W. Lim, D.-M. Kang, H.-K. Ahn, T.-H. Shin, J. Cheon, H.-S. Lee, R. Weissleder, C. M. Castro, H. Lee, *Lab on a Chip* **2017**, 17, 4000-4007.
- [77] S. Kamara, Q.-H. Tran, V. Davesne, G. Félix, L. Salmon, K. Kim, C. Kim, A. Bousseksou, F. Terki, *Adv. Mater.* **2017**, 29, 1703073.